Inorganic Chemistry
Article

Inorg. Chem. **2009**, *48*, 10177–10185 **10177**
DOI: 10.1021/ic901224f

One-Dimensional Homochiral Cyano-Bridged Heterometallic Chain Coordination Polymers with Metamagnetic or Ferroelectric Properties

He-Rui Wen,*,† Yun-Zhi Tang,† Cai-Ming Liu,*,‡ Jing-Lin Chen,† and Chang-Lin Yu†

†*School of Materials and Chemical Engineering, Jiangxi University of Science and Technology, Ganzhou 341000, China, and* ‡*Beijing National Laboratory for Molecular Sciences, Center for Molecular Science, Institute of Chemistry, Chinese Academy of Sciences, Beijing 100190, China*

Received June 25, 2009

Two couples of enantiomerically pure chiral cyano-bridged heterobimetallic chain coordination polymers, $[Mn((R,R)\text{-Salcy})Fe(Tp)(CN)_3\cdot H_2O\cdot 1/2CH_3CN]_n$ (**1**), $[Mn((S,S)\text{-Salcy})Fe(Tp)(CN)_3\cdot H_2O\cdot 1/2CH_3CN]_n$ (**2**), $[Mn((R,R)\text{-Salcy})Fe(bpca)(CN)_3\cdot H_2O]_n$ (**3**), and $[Mn((S,S)\text{-Salcy})Fe(bpca)(CN)_3\cdot H_2O]_n$ (**4**) [(*R*,*R*)-Salcy or (*S*,*S*)-Salcy = (*R*,*R*)- or (*S*,*S*)-N,N′-(1,2-cyclohexanediylethylene)bis(salicylideneiminato) dianion, Tp = tris(pyrazolyl)hydroborate, bpca = bis(2-pyridylcarbonyl)amidate anion], were synthesized using the modified cyanometalate building blocks $[Fe(L)(CN)_3]^-$ (L = Tp, bpca) and the chiral polydentate Schiff base manganese(III) complex fragments. The circular dichroism measurements showed Cotton effects of the opposite sign at the same wavelength for each pair of enantiomers. Magnetic property studies indicated that complexes **1** and **2** show not only intrachain but also interchain field-induced metamagnetic transitions from an antiferromagnetic to a ferromagnetic state and exhibit an antiferromagnetic long-range ordering with a T_N of 3.2 K, while enantiomers **3** and **4** are typical antiferromagnetic coupling compounds. Furthermore, complex **3** exhibits a ferroelectric behavior that relates to the polar point group C_2, in which it crystallizes.

Introduction

The continuously increasing demand for specific materials with potential applications has stimulated extensive research in the area of multifunctional materials.[1] The construction of molecule-based magnetic materials, which possess additional properties such as conductivity,[2] ferroelectricity,[3] chirality, and optical properties,[4] is an active field currently. When a magnet is characterized by the chiral structure, there is the possibility that it may have a chiral spin structure, and the magnet may display asymmetric magnetic anisotropy and magneto-chiral dichroism (MChD).[5] The concept of MChD was first mentioned by Barron and Vrbancich in 1984, for describing the relationship between the natural optical activity and the magnetic-field-induced circular dichroism.[6] Subsequently, Rikken and Raupach experimentally observed the MChD effect of the chiral paramagnetic compound, tris-(3-trifluoroacetyl-(±)-camphorato)europium(III).[5] On the other hand, the chirality may make the magnetic molecules crystallize in the polar point group, which is required for the ferroelectricity. Therefore, the synthesis and properties of chiral magnets are of continuous, increasing interest due to their potential important applications as multifunctional materials,[7] especially as multiferroic materials in which both the ferromagnetism and the ferroelectricity can coexist. The studies on multiferroic materials were mainly focused on pure inorganic compounds such as $RMnO_3$, RMn_2O_5

*To whom correspondence should be addressed. E-mail: wenhr@mail.jxust.cn (H.-R.W.), cmliu@iccas.ac.cn (C.-M.L.).

(1) Kahn, O. *Molecule Magnetism*; VCH: Weinhem, Germany, 1993.
(2) Coronado, E.; Galan-Mascaros, J. R.; Gomez-Garcia, C. J.; Laukhin, V. *Nature* **2000**, *408*, 447–449.
(3) (a) Spaldin, N. A.; Fiebig, M. *Science* **2005**, *309*, 391–392. (b) Sott, J. F. *Science* **2006**, *315*, 954–959. (c) Eerenstein, W.; Mathur, N. D.; Scott, J. F. *Nature* **2006**, *442*, 759–765. (d) Sott, J. F. *Nat. Mater.* **2007**, *6*, 256–257. (e) Ramesh, R.; Spaldin, N. A. *Nat. Mater.* **2007**, *6*, 21–29.
(4) Andres, R.; Brissard, M.; Gruselle, M.; Train, C.; Vaissermann, J.; Malezieux, B.; Jamet, J.-P.; Verdaguer, M. *Inorg. Chem.* **2001**, *40*, 4633–4640.
(5) Rikken, G. L. J. A.; Raupach, E. *Nature* **1997**, *390*, 493–494.
(6) Barron, L. D.; Vrbancich, J. *Mol. Phys.* **1984**, *51*, 715–730.
(7) (a) Sedó, J.; Ventosa, N.; Ruiz-Molina, D.; Mas, M.; Molins, E.; Rovira, C.; Veciana, J. *Angew. Chem., Int. Ed.* **1998**, *37*, 330–333. (b) Caneschi, A.; Gatteschi, D.; Rey, P.; Sessoli, R. *Inorg. Chem.* **1991**, *30*, 3936–3941. (c) Nakayama, K.; Ishida, T.; Takayama, R.; Hashizume, D.; Yasui, M.; Iwasaki, F.; Nogami, T. *Chem. Lett.* **1998**, 497–498. (d) Kumagai, H.; Inoue, K. *Angew. Chem., Int. Ed.* **1999**, *38*, 1601–1603. (e) Minguet, M.; Luneau, D.; Lhotel, E.; Villar, V.; Paulsen, C.; Amabilino, D. B.; Veciana, J. *Angew. Chem., Int. Ed.* **2002**, *41*, 586–589. (f) Gao, E. Q.; Yue, Y. F.; Bai, S. Q.; He, Z.; Yan, C. H. *J. Am. Chem. Soc.* **2004**, *126*, 1419–1429. (g) Coronado, E.; Palacio, F.; Veciana, J. *Angew. Chem., Int. Ed.* **2003**, *42*, 2570–2572. (h) Coronado, E.; Gómez-García, C. J.; Nuez, A.; Romero, F. M.; Waerenborgh, J. C. *Chem. Mater.* **2006**, *18*, 2670–2681. (i) Coronado, E.; Galán-Mascarós, J. R.; Gómez-García, C. J.; Murcia-Martínez, A. *Chem. Eur. J.* **2006**, *12*, 3484–3492. (j) Gu, Z. G.; Song, Y.; Zuo, J. L.; You, X. Z. *Inorg. Chem.* **2007**, *46*, 9522–9524.

Published on Web 09/25/2009

(R = rare earths), and La_2MMnO_6 (M = Co, Ni, Cu) before,[8] whereas the chiral molecule-based magnets supply a new approach to the designable multiferroic materials.[9] Nevertheless, the construction of chiral molecule-based magnets is still a great challenging target because the chirality must be controlled in the molecular structure as well as in the entire crystal structure.

Cyanide is an efficient and versatile mediator for magnetic coupling. The cyano-bridged bimetallic assemblies have been extensively investigated, owing to their rich magnetic behaviors,[10] including high-T_c magnets,[11] photo- and electromagnets,[12] piezomagnets,[13] and single-molecule[14] or single-chain magnets.[15] Recently, a strategy of using hexacyanometallic anions as bridging units to link magnetic metal ions partially blocked by chiral diamine ligands has been utlized to prepare the chiral ferromagnetic compounds.[16] Considering the Schiff base manganese(III) complex fragments also can react with the hexacyanometallic anions to construct cyano-bridged magnetic complexes,[17] we popularized this strategy to the chiral Schiff base systems and successfully prepared two one-dimensional enantiomerically pure chiral cyano-bridged heterobimetallic complexes, $[Mn_3((R,R)\text{-Salcy})_3(H_2O)_2Fe(CN)_6\cdot 2H_2O]_n$ and $[Mn_3((S,S)\text{-Salcy})_3(H_2O)_2Fe(CN)_6\cdot 2H_2O]_n$ [Salcy = N,N′-(1,2-cyclohexanediylethylene) bis(salicylideneiminato)dianion], quite recently, which exhibit ferrimagnetic behaviors.[18] To extend the cyano-bridged homochiral heterobimetallic molecule-based magnetic and ferroelectric materials based on the chiral Schiff base complex fragments, further studies have been carried out by employing the modified cyanometalates, $[Fe(TP)(CN)_3]^-$ and $[Fe(bpca)(CN)_3]^-$ [Tp = Tris(pyrazolyl)hydroborate, bpca = bis-(2-pyridylcarbonyl)amidate anion]. Herein, we report the synthesis, crystal structures, circular dichroism spectra, ferroelectric and magnetic properties of four enantiomerically pure chiral cyano-bridged heterobimetallic chain coordination polymers, $[Mn((R,R)\text{-Salcy})Fe(Tp)(CN)_3\cdot H_2O\cdot 1/2CH_3CN]_n$ (**1**), $[Mn((S,S)\text{-Salcy})Fe(Tp)(CN)_3\cdot H_2O\cdot 1/2CH_3CN]_n$ (**2**), $[Mn((R,R)\text{-Salcy})Fe(bpca)(CN)_3\cdot H_2O]_n$ (**3**), and $[Mn((S,S)\text{-Salcy})Fe(bpca)(CN)_3\cdot H_2O]_n$ (**4**). The bending degree of the corresponding Mn−N≡C bond angles in these two couples of enantiomers has a great influence on their magnetic properties. Furthermore, a ferroelectric property was observed for **3** (or **4**) because it crystallizes in the polar point group (C_2).

Experimental Section

Materials and Physical Measurements. All chemicals were reagent grade and used as received. (*R*,*R*)- and (*S*,*S*)-1,2-diaminocyclohexane were purchased form the Aldrich Chemical Co. $(Bu_4N)[(Tp)Fe(CN)_3]$,[19] $(Bu_4N)[(bpca)Fe(CN)_3]$,[20] and $[Mn((R,R)\text{-Salcy})(H_2O)_2]ClO_4$ and $[Mn((S,S)\text{-Salcy})(H_2O)_2]ClO_4$[14e] were prepared according to literature methods. Elemental analyses for C, H, and N were performed on a Perkin-Elmer 240C analyzer. Infrared spectra were recorded on a Vector22 Bruker spectrophotometer with KBr pellets in the 400−4000 cm^{-1} region. The circular dichroism spectra were recorded on a JASCO J-810 spectropolarimeter with KBr pellets. The ferroelectric property of the solid-state sample was measured as a pellet-covered silver-conductive glue on the Radiant Technologies Premier Precision II ferroelectric tester at room temperature. Variable-temperature magnetic susceptibility, zero-field ac magnetic susceptibility, and field dependence of magnetization were measured on a Quantum Design MPMSXL5 (SQUID) magnetometer. Diamagnetic corrections were estimated from Pascal's constants for all constituent atoms.

Preparation of $[Mn((R,R)\text{-Salcy})Fe(Tp)(CN)_3\cdot H_2O\cdot 1/2CH_3CN]_n$ (1). A total of 5 mL of an acetonitrile solution of $(Bu_4N)[(Tp)Fe(CN)_3]$ (0.10 mmol) was added to the solution of

(8) (a) Azuma, M.; Takata, K.; Saito, T.; Ishiwata, S.; Shimakawa, Y.; Takano, M. *J. Am. Chem. Soc.* **2005**, *127*, 8889–8892. (b) Khomskii, D. I. *J. Magn. Magn. Mater.* **2006**, *306*, 1–8. (c) Cheong, S. W.; Mostovoy, M. *Nat. Mater.* **2007**, *6*, 13–20. (d) Rao, C. N. R.; Serrao, C. R. *J. Chem. Mater.* **2007**, *17*, 4931–4938. (e) Jiang, Q. H.; Ma, J.; Lin, Y. H.; Nan, C. W.; Shi, Z.; Shen, Z. J. *Appl. Phys. Lett.* **2007**, *91*, 022914–022915.

(9) (a) Cui, H. B.; Wang, Z.; Takahashi, K.; Okano, Y.; Kobayashi, H.; Kobayashi, A. *J. Am. Chem. Soc.* **2006**, *128*, 15074–15075. (b) Ohkoshi, S.; Tokoro, H.; Matsuda, T.; Takahashi, H.; Irie, H.; Hashimoto, K. *Angew. Chem., Int. Ed.* **2007**, *46*, 3238–3241. (c) Gu, Z. G.; Zhou, X. H.; Jin, Y. B.; Xiong, R. G.; Zuo, J. L.; You, X. Z. *Inorg. Chem.* **2007**, *46*, 5462–5464. (d) Ye, Q.; Fu, D. W.; Tian, H.; Xiong, R. G.; Chan, P. W. H.; Huang, S. D. *Inorg. Chem.* **2008**, *47*, 772–774. (e) Wang, C. F.; Gu, Z. G.; Lu, X. M.; Zuo, J. L.; You, X. Z. *Inorg. Chem.* **2008**, *47*, 7957–7959.

(10) (a) Ohba, M.; Okawa, H. *Coord. Chem. Rev.* **2000**, *198*, 313–328. (b) Černák, J.; Orendáč, M.; Potočák, I.; Chomič, J.; Orendáčová, A.; Skoršepa, J.; Feher, A. *Coord. Chem. Rev.* **2002**, *224*, 51–66. (c) Beltran, L. M. C.; Long, J. R. *Acc. Chem. Res.* **2005**, *38*, 325–334.

(11) (a) Sato, O.; Iyoda, T.; Fujishima, A.; Hashimoto, K. *Science* **1996**, *271*, 49–51. (b) Holmes, S. M.; Girolami, G. S. *J. Am. Chem. Soc.* **1999**, *121*, 5593–5594. (c) Hatlevik, Ø.; Buschman, W. E.; Zhang, J.; Manson, J. L.; Miller, J. S. *Adv. Mater.* **1999**, *11*, 914–918.

(12) (a) Ohkoshi, S. I.; Fujishima, A.; Hashimoto, K. *J. Am. Chem. Soc.* **1998**, *120*, 5349–5350. (b) Sato, O.; Einaga, Y.; Fujishima, A.; Hashimoto, K. *Inorg. Chem.* **1999**, *38*, 4405–4412. (c) Arimoto, Y.; Ohkoshi, S. I.; Zhong, Z. J.; Seino, H.; Mizobe, Y.; Hashimoto, K. *J. Am. Chem. Soc.* **2003**, *125*, 9240–9241. (d) Sato, O. *Acc. Chem. Res.* **2003**, *36*, 692−700 and references therein.(e) Wang, C. F.; Gu, Z. G.; Lu, X. M.; Zuo, J. L.; You, X. Z. *Inorg. Chem.* **2008**, *47*, 7957–7959.

(13) Coronado, E.; Giménez-López, M. C.; Levchenko, G.; Romero, F. M.; García-Baonza, V.; Milner, A.; Paz-Pasternak, M. *J. Am. Chem. Soc.* **2005**, *127*, 4580–4581.

(14) (a) Sokol, J. J.; Hee, A. G.; Long, J. R. *J. Am. Chem. Soc.* **2002**, *124*, 7656–7657. (b) Berlinguette, C. P.; Vaughn, D.; Cañada-Vilalta, C.; Galán-Mascarós, J. R.; Dunbar, K. R. *Angew. Chem., Int. Ed.* **2003**, *42*, 1523–1526. (c) Schelter, E. J.; Prosvirin, A. V.; Dunbar, K. R. *J. Am. Chem. Soc.* **2004**, *126*, 15004–15005. (d) Wang, S.; Zuo, J. L.; Zhou, H. C.; Choi, H. J.; Ke, Y.; Long, J. R.; You, X. Z. *Angew. Chem., Int. Ed.* **2004**, *43*, 5940–5943. (e) Wang, C. F.; Zuo, J. L.; Bartlett, B. M.; Song, Y.; Long, J. R.; You, X. Z. *J. Am. Chem. Soc.* **2006**, *128*, 7162–7163.

(15) (a) Lescouëzec, R.; Vaissermann, J.; Ruiz-Pérez, C.; Lloret, F.; Carrasco, R.; Julve, M.; Verdaguer, M.; Dromzee, Y.; Gatteschi, D.; Wernsdorfer, W. *Angew. Chem., Int. Ed.* **2003**, *42*, 1483–1486. (b) Toma, L. M.; Lescouëzec, R.; Lloret, F.; Julve, M.; Vaissermann, J.; Verdaguer, M. *Chem. Commun.* **2003**, 1850–1851. (c) Wang, S.; Zuo, J. L.; Gao, S.; Song, Y.; Zhou, H. C.; Zhang, Y. Z.; You, X. Z. *J. Am. Chem. Soc.* **2004**, *126*, 8900–8901.

(16) (a) Inoue, K.; Imai, H.; Ghalsasi, P. S.; Kikuchi, K.; Ohba, M.; Okawa, H.; Yakhmi, J. V. *Angew. Chem., Int. Ed.* **2001**, *40*, 4242–4245. (b) Coronado, E.; Gómez-García, C. J.; Nuez, A.; Romero, F. M.; Rusanov, E.; Stoeckli-Evans, H. *Inorg. Chem.* **2002**, *41*, 4615–4617. (c) Inoue, K.; Kikuchi, K.; Ohba, M.; Okawa, H. *Angew. Chem., Int. Ed.* **2003**, *42*, 4810–4813. (d) Imai, H.; Inoue, K.; Kikuchi, K.; Yoshida, Y.; Ito, M.; Sunahara, T.; Onaka, S. *Angew. Chem., Int. Ed.* **2004**, *43*, 5618–5621.

(17) (a) Miyasaka, H.; Matsumoto, N.; Okawa, H.; Re, N.; Gallo, E.; Floriani, C. *Angew. Chem., Int. Ed.* **1995**, *34*, 1446–1448. (b) Re, N.; Gallo, E.; Floriani, C.; Miyasaka, H.; Matsumoto, N. *Inorg. Chem.* **1996**, *35*, 5964–5965. (c) Miyasaka, H.; Matsumoto, N.; Okawa, H.; Re, N.; Gallo, E.; Floriani, C. *J. Am. Chem. Soc.* **1996**, *118*, 981–994. (d) Miyasaka, H.; Matsumoto, N.; Re, N.; Gallo, E.; Floriani, C. *Inorg. Chem.* **1997**, *36*, 670–676. (e) Miyasaka, H.; Ieda, H.; Matsumoto, N.; Re, N.; Crescenzi, R.; Floriani, C. *Inorg. Chem.* **1998**, *37*, 255–263. (f) Re, N.; Crescenzi, R.; Floriani, C.; Miyasaka, H.; Matsumoto, N. *Inorg. Chem.* **1998**, *37*, 2717–2722. (g) Choi, H. J.; Sokol, J. J.; Long, J. R. *Inorg. Chem.* **2004**, *43*, 1606–1608. (h) Miyasaka, H.; Takahashi, H.; Madanbashi, T.; Sugiura, K. J.; Clerac, R.; Nojiri, H. *Inorg. Chem.* **2005**, *44*, 5969–5971. (i) Ferbinteanu, M.; Miyasaka, H.; Wernsdorfer, W.; Nakata, K.; Sugiura, K.-I.; Yamashita, M.; Coulon, C.; Clérac, R. *J. Am. Chem. Soc.* **2005**, *127*, 3090–3099.

(18) Wen, H. R.; Wang, C. F.; Li, Y. Z.; Zuo, J. L.; Song, Y.; You, X. Z. *Inorg. Chem.* **2006**, *45*, 7032–7034.

(19) Lescouëzec, R.; Vaissermann, J.; Lloret, F.; Julve, M.; Verdaguer, M. *Inorg. Chem.* **2002**, *41*, 5943–5945.

(20) Lescouëzec, R.; Vaissermann, J.; Toma, L. M.; Carrasco, R.; Lloret, F.; Julve, M. *Inorg. Chem.* **2004**, *43*, 2234–2236.

Table 1. Crystallographic Data for Complexes **1**−**4**

	1	**2**	**3**	**4**
empirical formula	$C_{66}H_{67}B_2Fe_2Mn_2N_{23}O_6$	$C_{66}H_{67}B_2Fe_2Mn_2N_{23}O_6$	$C_{35}H_{30}FeMnN_8O_5$	$C_{35}H_{30}FeMnN_8O_5$
fw	1521.63	1521.63	753.46	753.46
cryst syst	orthorhombic	orthorhombic	monoclinic	monoclinic
space group	$P2_12_12$	$P2_12_12$	$P2_1$	$P2_1$
a/Å	15.516(4)	15.490(3)	10.3396(15)	10.3411(13)
b/Å	24.754(5)	24.726(5)	13.2455(19)	13.2280(17)
c/Å	9.170(2)	9.1639(18)	11.8273(17)	11.8306(15)
α/deg	90	90	90	90
β/deg	90	90	92.361(3)	92.314(3)
γ/deg	90	90	90	90
V/Å^3	3521.8(13)	3509.8(12)	1618.4(4)	1617.0(4)
Z	2	2	2	2
ρ (calcd)/g cm^{-3}	1.435	1.440	1.546	1.547
T/K	293(2)	293(2)	291(2)	291(2)
μ, mm^{-1}	0.822	0.825	0.896	0.897
F(000)	1568	1568	774	774
index ranges	$-19 \le h \le +19$	$-20 \le h \le +17$	$-12 \le h \le +12$	$-12 \le h \le +12$
	$-26 \le k \le +31$	$-32 \le k \le +32$	$-16 \le k \le +16$	$-16 \le k \le +16$
	$-9 \le l \le +11$	$-10 \le l \le +12$	$-14 \le l \le +10$	$-13 \le l \le +14$
data/restraints/ params	7316/0/459	8190/0/492	6285/3/454	6002/1/451
GOF (F^2)	1.089	1.057	1.053	1.057
R_1, wR_2 ($I > 2\sigma(I)$)	0.0634, 0.1378	0.0754, 0.1849	0.0632, 0.1325	0.0640, 0.1402
R_1, wR_2 (all data)	0.0737, 0.1409	0.0944, 0.1918	0.0770, 0.1359	0.0758, 0.1434
largest diff. peak and hole (e Å^{-3})	0.359 and −0.405	0.363 and −2.934	0.322 and −0.612	0.297 and −0.577

[Mn((*R*,*R*)-Salcy)$(H_2O)_2$]ClO_4 (0.10 mmol) in 5 mL of acetonitrile. Slow evaporation of the resulting solution at room temperature afforded brown-black crystals of **1** after a week. Yield: 75%. Anal. Calcd for $C_{66}H_{67}B_2Fe_2Mn_2N_{23}O_6$: C, 52.05; H, 4.40; N, 21.16. Found: C, 52.16; H, 4.33; N, 21.02. IR (KBr, cm^{-1}): 2128 (ν_{-CN}) and 2146 ($\nu_{\mu\text{-CN}}$).

Preparation of [Mn((*S*,*S*)-Salcy)Fe(Tp)$(CN)_3\cdot H_2O\cdot 1/2CH_3CN$]$_n$ (2). Complex **2** was prepared in a procedure similar to that for **1**, except that [Mn((*S*,*S*)-Salcy)$(H_2O)_2$]ClO_4 was used. Yield: 70%. Anal. Calcd for $C_{66}H_{67}B_2Fe_2Mn_2N_{23}O_6$: C, 52.05; H, 4.40; N, 21.16. Found: C, 52.17; H, 4.35; N, 21.01. IR (KBr, cm^{-1}): 2128 (ν_{-CN}) and 2146 ($\nu_{\mu\text{-CN}}$).

Preparation of [Mn((*R*,*R*)-Salcy)Fe(bpca)$(CN)_3\cdot H_2O$]$_n$ (3). A total of 10 mL of an acetonitrile solution of (Bu_4N)[(bpca)Fe$(CN)_3]\cdot H_2O$ (0.10 mmol) was added to the solution of [Mn((*R*,*R*)-Salcy)$(H_2O)_2$]ClO_4 (0.10 mmol) in 5 mL of methanol. Slow evaporation of the resulting solution at room temperature afforded black crystals of **3** after a week. Yield: 75%. Anal. Calcd for $C_{35}H_{30}FeMnN_8O_5$: C, 55.74; H, 3.98; N, 14.86. Found: C, 55.33; H, 3.87; N, 15.01. IR (KBr, cm^{-1}): 2118(ν_{-CN}) and 2130 ($\nu_{\mu\text{-CN}}$).

Preparation of [Mn((*S*,*S*)-Salcy)Fe(bpca)$(CN)_3\cdot H_2O$]$_n$ (4). Complex **4** was afforded in a similar procedure to that for **3**, except that [Mn((*S*,*S*)-Salcy)$(H_2O)_2$]ClO_4 was used. Yield: 70%. Anal. Calcd for $C_{35}H_{30}FeMnN_8O_5$: C, 55.74; H, 3.98; N, 14.86. Found: C, 56.25; H, 3.91; N, 14.87. IR (KBr, cm^{-1}): 2118 (ν_{-CN}) and 2130 ($\nu_{\mu\text{-CN}}$).

X-Ray Crystallography Measurements. The crystal structures of complexes **1**−**4** were determined on a Bruker SMART CCD diffractometer using monochromated Mo Kα radiation (λ = 0.71073 Å). Absorption corrections were applied using SADABS supplied by Bruker. Structures were solved by direct methods using the program SHELXTL-97. The positions of the metal atoms and their first coordination spheres were located from direct-methods *E*-maps; other non-hydrogen atoms were found using alternating difference Fourier syntheses and least-squares refinement cycles and, during the final cycles, were refined anisotropically. Hydrogen atoms were placed in calculated position and refined as riding atoms with a uniform value of U_{iso}. A summary of the crystal data collection and refinement parameters is given in Table 1. Selected bond lengths and angles are given in Tables 2 (for enantiomers **1** and **2**) and 3 (for enantiomers **3** and **4**).

Results and Discussion

Syntheses and Spectroscopic Studies. Compounds **1**−**4** were prepared by the reaction of (Bu_4N)[(Tp)Fe$(CN)_3$] or (Bu_4N)[(bpca)Fe$(CN)_3$] with [Mn((*R*,*R*)-Salcy)$(H_2O)_2$]ClO_4 or [Mn((*S*,*S*)-Salcy)$(H_2O)_2$]ClO_4 in a 1:1 molar ratio in acetonitrile or a mixture of acetonitrile and methanol at room temperature. The IR spectra show that there are two sharp peaks of medium intensity (2128 and 2146 cm^{-1} for **1** and **2** and 2117 and 2129 cm^{-1} for **3** and **4**) observed in the C≡N stretching region, which are consistent with the presence of both terminal and bridging cyanide groups. The circular dichroism (CD) spectra in KBr pellets were measured to confirm the optical activity and the enantiomeric nature of these compounds. The CD spectrum of complex **1** (*R*,*R* isomer) exhibits a strong negative Cotton effect at λ = 325 nm and a positive dichroic signal centered at λ = 600 nm, while complex **2** (*S*,*S* isomer) shows Cotton effects of the opposite sign at the same wavelengths (Figure 1). The CD spectrum of complex **3** (*R*,*R* isomer) exhibits a positive Cotton effect at λ = 300, 350, and 600 nm and a negative dichroic signal centered at λ = 325 nm, while complex **4** (*S*,*S* isomer) shows Cotton effects of the opposite sign at the same wavelengths (Figure 2). These Cotton effect peaks can be assigned to the charge-transfer and *d*−*d* transitions of the UV/vis absorption spectra of these complexes, respectively.

Crystal Structures. Complexes **1**−**4** are characterized by X-ray crystallography. Complexes **1** and **2** are enantiomers and crystallized in the chiral space group $P2_12_12$. Since **1** and **2** are a pair of enantiomers, and they have similar crystal structures, only the crystal structure of **1** is described in detail here. As shown in Figure 3, coordination polymer **1** consists of the asymmetric chiral unit of [(Mn(*R*,*R*)-Salcy)Fe(Tp)$(CN)_3$]. Each [Fe(Tp)$(CN)_3]^-$ provides two fac cyanide groups to bridge two [Mn((*R*,*R*)-Salcy)]$^+$ units, generating an interesting $-Mn^{III}-NC-Fe(Tp)^{III}-CN-Mn^{III}-$ one-dimensional zigzag chain structure (Figure 4). The local

Table 2. Selected Bond Lengths (Å) and Angles (deg) for Complexes **1** and **2**

1 (#1 $x - 1/2, -y + 3/2, -z + 1$; #2 $x + 1/2, -y + 3/2, -z + 1$)

C(10)−Fe(1)	1.945(6)	Fe(1)−N(5)	1.985(4)	Mn(1)−O(2)	1.858(4)
C(11)−Fe(1)	1.939(5)	C(10)−N(7)	1.118(7)	Mn(1)−N(8)	2.281(5)
C(12)−Fe(1)	1.889(5)	C(11)−N(9)#1	1.156(7)	Mn(1)−N(9)	2.308(5)
Fe(1)−N(3)	1.959(4)	C(12)−N(8)	1.167(6)	Mn(1)−N(10)	1.986(4)
Fe(1)−N(1)	1.979(4)	Mn(1)−O(1)	1.862(4)	Mn(1)−N(11)	1.991(4)
N(7)−C(10)−Fe(1)	177.8(6)	C(12)−Fe(1)−N(5)	177.32(18)	O(2)−Mn(1)−N(8)	95.72(16)
N(9)#1−C(11)−Fe(1)	174.0(4)	C(11)−Fe(1)−N(5)	91.55(18)	O(1)−Mn(1)−N(8)	90.69(15)
N(8)−C(12)−Fe(1)	177.6(4)	C(10)−Fe(1)−N(5)	91.9(2)	N(10)−Mn(1)−N(8)	83.38(16)
C(12)−Fe(1)−C(11)	91.03(19)	N(3)−Fe(1)−N(5)	88.01(19)	N(11)−Mn(1)−N(8)	86.06(16)
C(12)−Fe(1)−C(10)	87.5(2)	N(1)−Fe(1)−N(5)	87.84(17)	O(2)−Mn(1)−N(9)	91.69(16)
C(11)−Fe(1)−C(10)	87.8(2)	O(2)−Mn(1)−O(1)	95.78(14)	O(1)−Mn(1)−N(9)	88.60(15)
C(12)−Fe(1)−N(3)	92.70(19)	O(2)−Mn(1)−N(10)	174.54(16)	N(10)−Mn(1)−N(9)	89.24(16)
C(11)−Fe(1)−N(3)	90.6(2)	O(1)−Mn(1)−N(10)	89.62(16)	N(11)−Mn(1)−N(9)	93.68(16)
C(10)−Fe(1)−N(3)	178.4(2)	O(2)−Mn(1)−N(11)	91.79(14)	N(8)−Mn(1)−N(9)	172.59(16)
C(12) Fe(1)−N(1)	89.58(18)	O(1)−Mn(1)−N(11)	172.02(16)	C(12)−N(8)−Mn(1)	162.8(4)
C(10)−Fe(1)−N(1)	91.8(2)	N(10)−Mn(1)−N(11)	82.78(16)	C(11)#2−N(9)−Mn(1)	149.5(4)
N(3)−Fe(1)−N(1)	89.72(17)				

2 (#1 $x + 1/2, -y - 1/2, -z - 1$ #2 $x - 1/2, -y - 1/2, -z - 1$)

C(10)−Fe(1)	1.913(6)	Fe(1)−N(3)	1.982(5)	Mn(1)−O(1)	1.876(3)
C(11)−Fe(1)	1.920(6)	C(10)−N(8)	1.150(7)	Mn(1)−N(11)	1.986(4)
C(12)#1−Fe(1)	1.913(6)	C(11)−N(7)	1.129(8)	Mn(1)−N(10)	1.989(5)
Fe(1)−N(1)	1.960(5)	C(12)−N(9)	1.128(7)	Mn(1)−N(9)	2.293(5)
Fe(1)−N(5)	1.971(4)	Mn(1)−O(2)	1.870(4)	Mn(1)−N(8)	2.317(5)
N(8)−C(10)−Fe(1)	174.6(5)	C(11)−Fe(1)−N(3)	92.7(3)	O(2)−Mn(1)−N(8)	93.06(18)
N(7)−C(11)−Fe(1)	176.9(6)	N(1)−Fe(1)−N(3)	87.6(2)	O(1)−Mn(1)−N(8)	88.93(18)
N(9)−C(12)−Fe(1)#2	176.0(5)	N(5)−Fe(1)−N(3)	88.02(19)	N(11)−Mn(1)−N(8)	93.46(18)
C(12)#1−Fe(1)−C(10)	91.0(2)	O(2)−Mn(1)−O(1)	95.55(16)	N(10)−Mn(1)−N(8)	88.34(12)
C(12)#1−Fe(1)−C(11)	87.2(3)	O(2)−Mn(1)−N(11)	91.96(17)	N(9)−Mn(1)−N(8)	88.34(19)
C(10)−Fe(1)−C(11)	88.1(3)	O(1)−Mn(1)−N(11)	171.99(17)	C(1)−N(1)−Fe(1)	133.8(5)
C(12)#1−Fe(1)−N(1)	92.4(2)	O(2)−Mn(1)−N(10)	174.08(19)	N(2)−N(1)−Fe(1)	119.9(3)
C(10)−Fe(1)−N(1)	90.3(2)	O(1)−Mn(1)−N(10)	90.22(18))	C(4)−N(3)−Fe(1)	132.3(4)
C(11)−Fe(1)−N(1)	178.4(2)	N(11)−Mn(1)−N(10)	82.2(2)	N(4)−N(3)−Fe(1)	119.1(4)
C(12)#1−Fe(1)−N(5)	90.1(2)	O(2)−Mn(1)−N(9)	94.78(16)	C(7)−N(5)−Fe(1)	134.2(4)
C(10)−Fe(1)−N(5)	178.9(2)	O(1)−Mn(1)−N(9)	90.26(17)	N(6)−N(5)−Fe(1)	119.4(3)
C(11)−Fe(1)−N(5)	92.1(2)	N(11)−Mn(1)−N(9)	86.33(17)	C(10)−N(8)−Mn(1)	149.8(4)
N(1)−Fe(1)−N(5)	89.5(2)	N(10)−Mn(1)−N(9)	83.87(18)	C(12)−N(9)−Mn(1)	161.5(4)
C(12)#1−Fe(1)−N(3)	178.1(2)				

coordination environment around the Fe(III) ion can be best described as a slightly distorted octahedron composed by three carbon atoms from cyanide groups and three nitrogen atoms from different pyrazolyl groups. Also, the Mn(III) ion adopts the same coordination mode, which coordinated by two opposite cyanide groups, two iminonitrogen atoms, and two phenolic oxygen atoms from the Schiff base. The C≡N−Mn bond angles are in the range of 149.50(4)−162.80(4)°, significantly deviating from 180°. The apical bond lengths of Mn−N [2.281(5)−2.308(5) Å] are longer than the equatorial bond lengths of Mn−N [1.986(4)−1.991(4) Å] and Mn−O [1.858(4)−1.862(4) Å] in the Mn(III) coordination environment, which indicates that the Mn(III) ion has an elongated and distorted octahedral coordination geometry. Such a clear Jahn−Teller axial elongation is expected for the high-spin d^4 Mn^{3+} ion in the distorted octahedral geometry. Double coedge six-membered rings and one coedge five-membered ring are formed along the bond sequences Mn1−O1−C18−C13−C19−N10−Mn1, Mn1−O2−C32−C27−C26−N11−Mn1, and Mn1−N1−C25−C20−N10−Mn1 by the chelating nitrogen and oxygen atoms from the Schiff base ligands (Figure 3). Also, in complex **2**, all of the central metal ions adopt the same coordination mode as that in complex **1** (Figure S1, Supporting Information). The chiral chair form of the 1,2-cyclohexane group induces the chiral structure of **1**. The intrachain Fe···Mn distances through the cyanide bridges are 5.2880(10) Å for $Fe1^{\#1}\cdots Mn1$ (#1 $0.5 + x$, $1.5 - y$, $1 - z$) and 5.1688(16) Å for Fe1···Mn1 in complex **1**. Complexes **1** and **2** are a pair of racemic compounds, and their imaging structures are shown in Figure 4. There is an intermolecular hydrogen bond between the solvent hydrate molecule and the nonbridged cyanide group with an O3···N7 distance of 2.804 Å and 2.770 Å for **1** and **2**, respectively. In addition, there exists another intermolecular hydrogen bond between the solvent water molecules with an $O3\cdots O3^{\#1}$ (# $1 - x$, $1 - y$, z) distance of 2.087 Å and 2.377 Å for **1** and **2**, respectively. These weak interactions extend the structures of **1** and **2** into 2D layer supramolecular arrays, which will impact the magnetic properties of **1** and **2**.

Complexes **3** and **4** are also enantiomers but crystallize in another chiral space group $P2_1$. Since they have similar crystal structures, no detailed descriptions are presented here for **4**. X-ray structural analyses show that the 1D coordination polymer consists of the asymmetric chiral unit of [(Mn(*R*,*R*)-Salcy)Fe(bpca)$(CN)_3$] for **3** and [(Mn(*S*,*S*)-Salcy)Fe(bpca)$(CN)_3$] for **4**, respectively. As shown in Figure 5, each $[Fe(bpca)CN]_3]^-$ anion provides two apical cyanide groups to bridge two $[Mn((R,R)\text{-Salcy})]^+$ cations to generate an infinite $-Mn^{III}-NC-Fe(bpca)^{III}-CN-Mn^{III}-$ one-dimensional zigzag chain structure (Figure 6). The local coordination environments around the Fe(III) ion and Mn(III) ion in **3** are the same as those in

Table 3. Selected Bond Lengths (Å) and Angles (deg) for Complexes **3** and **4**

3 (#1 $x-1, y, z$; #2 $x+1, y, z$)

C(1)−Fe(1)	1.9514(18)	Fe(1)−N(1)	1.9606(16)	Mn(1)−O(3)	1.8897(14)
C(2)−Fe(1)	1.9402(19)	C(1)−N(4)	1.148(2)	Mn(1)−N(7)	1.9732(15)
C(3)−Fe(1)	1.9241(16)	C(3)−N(6)	1.146(2)	Mn(1)−N(8)	1.9738(18)
Fe(1)−N(2)	1.8786(18)	C(2)−N(5)	1.145(3)	Mn(1)−N(4)	2.3132(16)
Fe(1)−N(3)	1.955(2)	Mn(1)−O(4)	1.8917(13)	Mn(1)−N(6)#1	2.3440(15)
N(4)−C(1)−Fe(1)	174.17(17)	C(1)−Fe(1)−N(3)	93.03(7)	O(4)−Mn(1)−N(4)	89.04(6)
N(5)−C(2)−Fe(1)	174.99(17)	N(2)−Fe(1)−N(1)	82.78(7)	O(3)−Mn(1)−N(4)	92.27(6)
N(6)−C(3)−Fe(1)	178.13(16)	C(3)−Fe(1)−N(1)	89.02(7)	N(7)−Mn(1)−N(4)	98.32(6)
N(2)−Fe(1)−C(3)	96.01(7)	C(2)−Fe(1)−N(1)	98.60(7)	N(8)−Mn(1)−N(4)	87.43(6)
N(2)−Fe(1)−C(2)	178.58(8)	C(1)−Fe(1)−N(1)	89.64(7)	O(4)−Mn(1)−N(6)#1	88.05(5)
C(3)−Fe(1)−C(2)	84.40(7)	N(3)−Fe(1)−N(1)	166.33(7)	O(3)−Mn(1)−N(6)#1	89.74(6)
N(2)−Fe(1)−C(1)	93.70(7)	O(4)−Mn(1)−O(3)	94.88(6)	N(7)−Mn(1)−N(6)#1	84.35(6)
C(3)−Fe(1)−C(1)	169.94(7)	O(4)−Mn(1)−N(7)	169.69(6)	N(8)−Mn(1)−N(6)#1	90.88(6)
C(2)−Fe(1)−C(1)	85.95(8)	O(3)−Mn(1)−N(7)	92.06(6)	N(4)−Mn(1)−N(6)#1	176.59(6)
N(2)−Fe(1)−N(3)	83.67(7)	O(4)−Mn(1)−N(8)	91.69(6)	C(1)−N(4)−Mn(1)	147.69(15)
C(3)−Fe(1)−N(3)	90.62(7)	O(3)−Mn(1)−N(8)	173.42(6)	C(3)−N(6)−Mn(1)#2	147.78(14)
C(2)−Fe(1)−N(3)	94.96(7)	N(7)−Mn(1)−N(8)	81.48(6)		

4 (#1 $x-1, y, z$; #2 $x+1, y, z$)

C(1)−Fe(1)	1.9553(18)	C(1)−N(4)	1.129(2)	Mn(2)−N(8)	1.9786(17)
C(2)−Fe(1)	1.9570(19)	C(2)−N(5)	1.146(3)	Mn(2)−N(7)	1.9818(18)
C(3)−Fe(1)	1.9676(18)	C(3)−N(6)	1.156(2)	Mn(2)−N(6)#1	2.2916(18)
Fe(1)−N(2)	1.8911(17)	Mn(2)−O(4)	1.8880(14)	Mn(2)−N(4)	2.3261(16)
Fe(1)−N(1)	1.9751(15)	Mn(2)−O(3)	1.8913(13)	N(6)−Mn(2)#2	2.2916(18)
Fe(1)−N(3)	1.988(2)				
N(4)−C(1)−Fe(1)	177.45(16)	C(3)−Fe(1)−N(1)	90.24(7)	O(4)−Mn(2)−N(6)#1	92.13(7)
N(5)−C(2)−Fe(1)	174.92(19)	N(2)−Fe(1)−N(3)	84.05(8)	O(3)−Mn(2)−N(6)#1	89.74(6)
N(6)−C(3)−Fe(1)	173.21(16)	C(1)−Fe(1)−N(3)	90.42(7)	N(8)−Mn(2)−N(6)#1	98.11(6)
N(2)−Fe(1)−C(1)	96.35(7)	C(2)−Fe(1)−N(3)	94.54(8)	N(7)−Mn(2)−N(6)#1	88.41(7)
N(2)−Fe(1)−C(2)	178.60(8)	C(3)−Fe(1)−N(3)	92.22(7)	O(4)−Mn(2)−N(4)	88.84(6)
C(1)−Fe(1)−C(2)	83.66(8)	N(1)−Fe(1)−N(3)	167.14(7)	O(3)−Mn(2)−N(4)	87.92(6)
N(2)−Fe(1)−C(3)	93.07(7)	O(4)−Mn(2)−O(3)	94.72(6)	N(8)−Mn(2)−N(4)	84.13(6)
C(1)−Fe(1)−C(3)	170.44(7)	O(4)−Mn(2)−N(8)	91.10(6)	N(7)−Mn(2)−N(4)	90.88(6)
C(2)−Fe(1)−C(3)	86.97(8)	O(3)−Mn(2)−N(8)	170.05(6)	N(6)#1−Mn(2)−N(4)	177.54(6)
N(2)−Fe(1)−N(1)	83.22(8)	O(4)−Mn(2)−N(7)	173.57(7)	C(1)−N(4)−Mn(2)	148.75(15)
C(1)−Fe(1)−N(1)	89.22(7)	O(3)−Mn(2)−N(7)	91.69(7)	C(3)−N(6)−Mn(2)#2	147.26(15)
C(2)−Fe(1)−N(1)	98.19(8)	N(8)−Mn(2)−N(7)	82.47(7)		

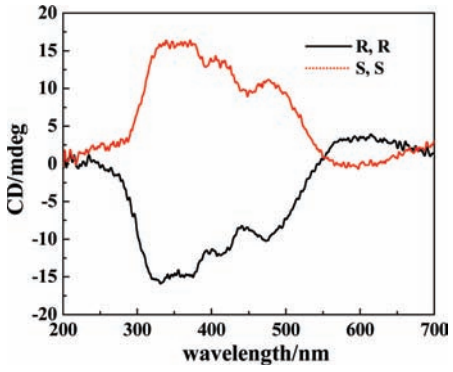

Figure 1. Circular dichroism spectra of complexes **1** (*R*,*R* isomer, solid) and **2** (*S*,*S* isomer, dash) in KBr pellets.

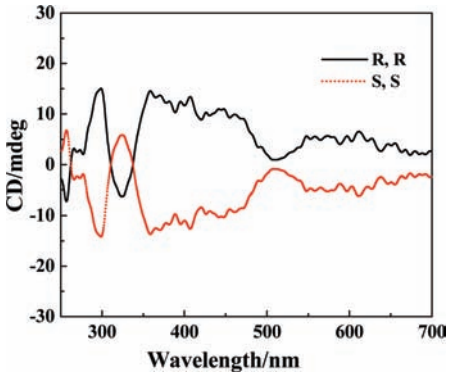

Figure 2. Circular dichroism spectra of complexes **3** (*R*,*R* isomer, solid) and **4** (*S*,*S* isomer, dash) in KBr pellets.

complex **1** and have a slightly distorted octahedron geometry. The C≡N−Mn bond angles are in the range of 147.26(15)−148.75(15)°, which are obviously smaller than those of complex **1**, indicating that the C≡N−Mn bond angles in complex **3** are bending more with respect to complex **1**. The cyano-bridged bond lengths of Mn−N are in the range of 2.3132(16)−2.3440(15) Å, which are slightly longer than those of complex **1**. The apical Mn−N bond lengths [2.3132(16)−2.3440(15) Å] are longer than the Mn−N bond lengths [1.9732(18)−1.9738(18) Å] and the Mn−O bond lengths [1.8917(13)−1.8897(14) Å] in the equator, owing to the Jahn−Teller effect. The chiral chair form of the 1,2-cyclohexane group leads to the chiral structure of **3**. The intrachain Fe···Mn distances through the cyanide bridges are 5.1972(8) Å for Fe1···Mn1$^{\#2}$ (#2 $1+x, y, z$) and 5.1622(8) Å for Fe1···Mn1 in **3**, which are a little shorter than those in **1**. The imaging structures of complexes **3** and **4** are shown in Figure 6.

Ferroelectric Properties. Since **3** and **4** crystallize in a point group (C_2) that is one of the 10 polar point groups (C_1, C_s, C_2, C_{2v}, C_4, C_{4v}, C_3, C_{3v}, C_6, and C_{6v}) required for ferroelectric behavior, their ferroelectric properties were

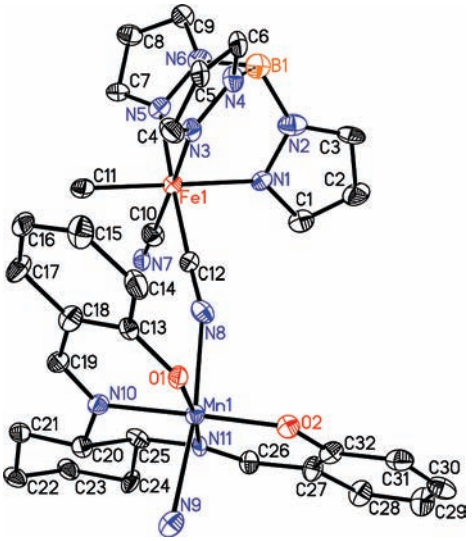

Figure 3. An ORTEP view of the structure segment of **1** showing the 30% probability thermal ellipsoid and atom-numbering scheme. The hydrogen atoms and solvent molecules are omitted for clarity.

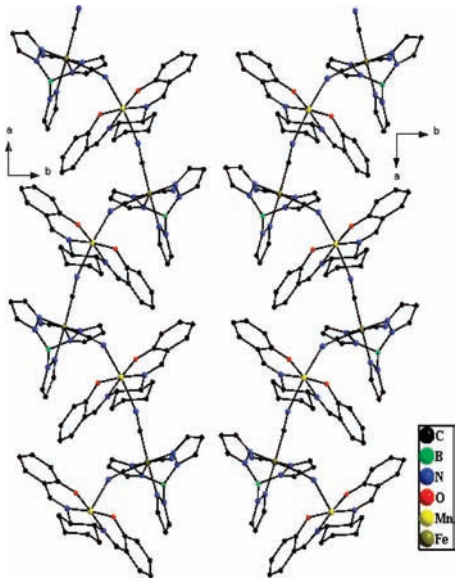

Figure 4. The one-dimensional zigzag infinite linear structures of **1** (*R*,*R* isomer, right) and **2** (*S*,*S* isomer, left).

investigated. Because **3** and **4** constitute a pair of enantiomers, they exhibit similar physical properties, and only the ferroelectric properties of **3** are described in detail here. An extremely low leakage current (less than 10^{-8} A cm^{-2}; Figure S3 in the Supporting Information) and ferroelectric hysteresis loops (Figure 7) were observed. The $E-P$ hysteresis loops show a typical ferroelectric feature with a coercive field (E_c) of ca. 3.8−12.0 kV cm^{-1} and a remanent polarization (P_r) of ca. 0.05−0.15 μC cm^{-2} at a 23.0−38.5 kV·cm^{-1} applied field, and the ferroelectric behavior is similar to that of the cyano-bridged trinulear heterobimetallic linear compound $\{(MeTp)_2Fe_2(CN)_6Ni[(1R,2R)\text{-chxn}]_2\}$ [chxn = 1,2-diaminocyclohexane; MeTp = methyltris(pyrazolyl)borate] reported quite recently.[9e] Compound **3** consists of the chiral $[Mn((R,R)\text{-Salcy})]^+$ and $[Fe(bpca)\text{-}CN]_3]^-$ units. Not only the Fe(III) but also the Mn(III) ions have a distorted asymmetric octahedron coordination

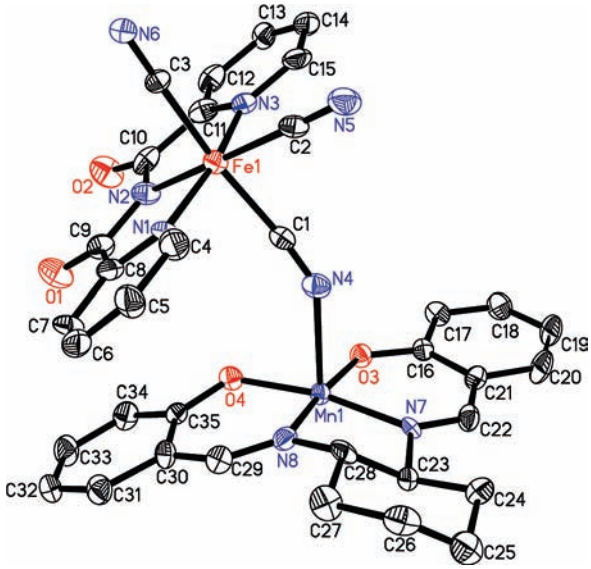

Figure 5. An ORTEP view of the structure segment of **3** showing the 30% probability thermal ellipsoid and atom-numbering scheme. The hydrogen atoms and solvent molecules are omitted for clarity.

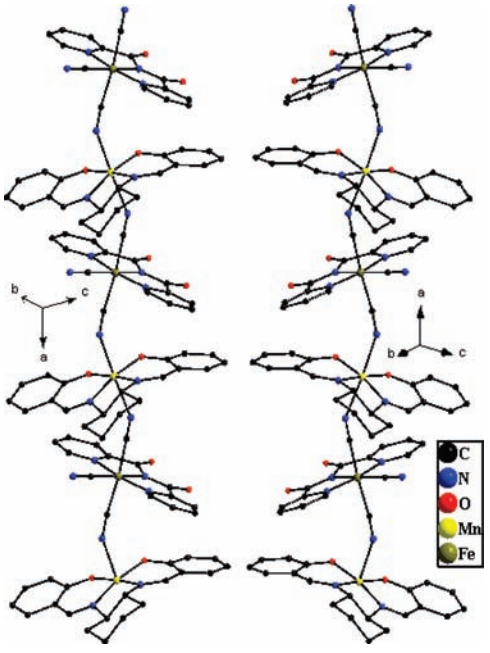

Figure 6. The one-dimensional zigzag infinite linear structures of **3** (*R*,*R* isomer, right) and **4** (*S*,*S* isomer, left).

environment, and the bpca, cyanide, and Schiff base ligands around the Fe(III) and Mn(III) ions are all highly polar molecules. In addition, the Mn(III) Jahn−Teller distortion enhances the local structural distortion, for example, the obvious deviation of the cyano-bridged bond angle Mn−N≡C from 180°. Probably, in such a deviated structure, polarization will be induced by the applied electric field. So, the ferroelectricity may result from the highly distorted structures with strongly local dipole groups in the molecule.[9b,21]

(21) (a) Lu, Y. Y.; Claud, J.; Neese, B.; Zhang, Q. M.; Wang, Q. *J. Am. Chem. Soc.* **2006**, *128*, 8120–8121. (b) Chung, T. C.; Petchsuk, A. *Macromolecules* **2002**, *35*, 7678–7684.

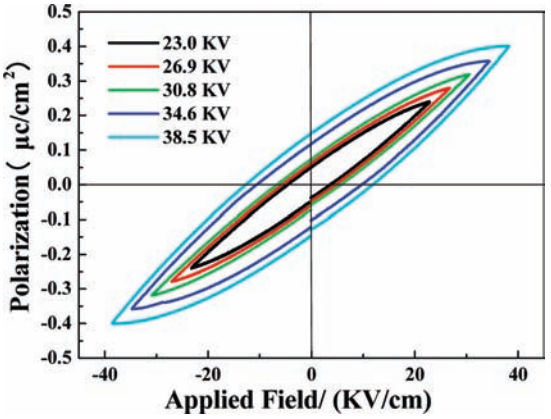

Figure 7. Electric hysteresis loop of a pellet of powders of **3** at different electric fields.

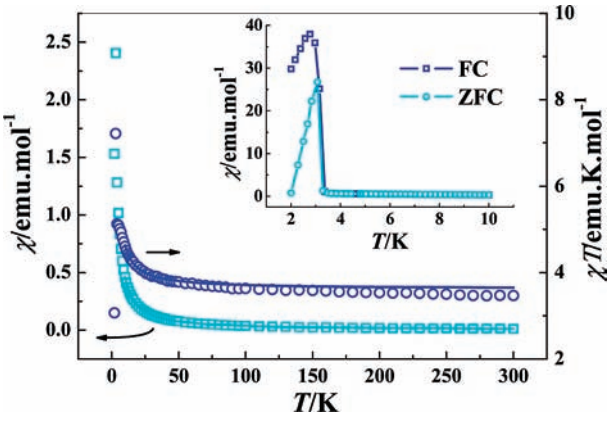

Figure 8. Temperature dependence of magnetic susceptibility in the forms of χT and χ vs T for **1** at 1000 Oe. The solid lines represent the best theoretical fitting. ZFC and FC susceptibility plots (inset).

Magnetic Properties. The magnetic measurements were performed on polycrystalline samples of complexes **1**−**4** using a SQUID magnetometer. The temperature dependence of $\chi_{mol}T$ values of complex **1** at 1000 Oe is displayed in Figure 8. The $\chi_{mol}T$ value is 3.48 emu K mol^{-1} at 300 K, which is close to the spin-only value of 3.43 emu K mol^{-1} based on the MnFe unit ($S_{Mn} = 2$, $S_{Fe} = 1/2$, $g_{Mn} = 2$, $g_{Fe} = 2.17$). As the temperature decreases, the $\chi_{mol}T$ product gradually increases, indicating the weak ferromagnetic coupling between the Mn^{III} and Fe^{III} ions in complex **1**. At 3 K, it jumps up to a maximum value of 7.22 emu K mol^{-1}, suggesting the commencement of magnetic ordering. Upon further cooling, the $\chi_{mol}T$ value abruptly decreases to 3.06 emu K mol^{-1} at 2 K, which may arise from zero-field splitting, Zeeman effects, or weak interchain interactions. The susceptibility data above 10 K were well-fitted to the Curie−Weiss law, with $C = 3.44$ cm^3 mol^{-1} K and $\Theta = 4.14$ K. An expression for the Heisenberg linear chain with spin alternation derived by Drillon et al.[22a] was utilized to fit the susceptibility, giving $J = 1.20$ cm^{-1}, $g_{Mn} = 2.05$, and $g_{Fe} = 2.11$, with $R = 8.7 \times 10^{-4}$. Only data for temperatures above 10 K were considered in the fit to preclude interchain

(22) (a) Drillon, M.; Coronado, E.; Beltran, D.; Georges, R. *Chem. Phys.* **1983**, *79*, 449–453. (b) Kim, J. I.; Yoo, H. S.; Koh, E. K.; Hong, C. S. *Inorg. Chem.* **2007**, *46*, 10461–10463.

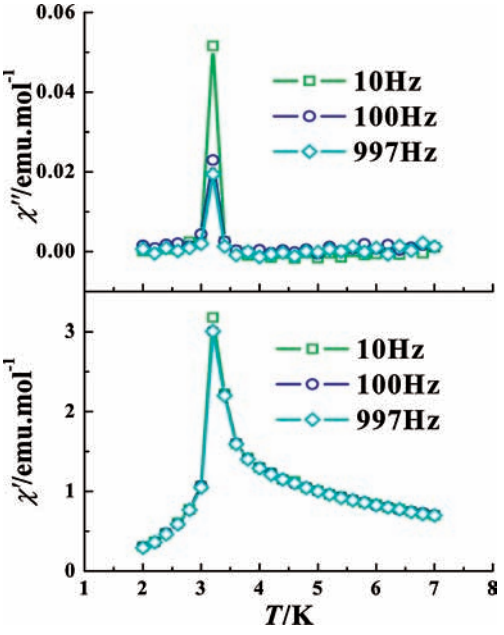

Figure 9. The ac magnetic susceptibility as a function of temperature for **1** at different frequencies and $H_{ac} = 2.5$ Oe and $H_{dc} = 0$ Oe.

interaction and the zero-field-splitting effect.[22b] The small positive J_{MnFe} value indicates the weak ferromagnetic coupling between the Mn^{III} and Fe^{III} ions mediated by the cyanide bridge.

The divergence of the field-cooled (FC) and the zero-field-cooled (ZFC) susceptibility $\chi_{mol}(T)$ data around 3.2 K confirms the irreversible behavior of long-range magnetic order (Figure 8, inset, shown as χ_{mol} versus T plots). There is a peak at about 3.2 K in the ZFC curve, corresponding to the Neel temperature, a critical temperature for the antiferromagnetic long-range order. The ac susceptibility measurements show that both the real (χ_{ac}') and imaginary parts (χ_{ac}'') of ac magnetic susceptibility are frequency-independent and have a peak at the low temperature of 3.2 K for frequencies of 10, 100, and 997 Hz, confirming the existence of magnetic ordering (Figure 9). This peak indicates that T_N is exactly 3.2 K, and small parts of the antiferromagnetic domains make a canting arrangement to produce a spontaneous magnetization.

Further magnetic investigations reveal that there are two field-induced magnetic transitions for **1**, which corresponds to a valley at about 1000 Oe and a peak at about 8100 Oe in the dM/dH versus H curve (Figure 10, inset). The temperature dependence of the magnetic susceptibility at various fields is shown in Figure 11. At a low field of 500 Oe, the $\chi_{mol}T$ product gradually decreases upon cooling and reaches a minimum at 4 K, suggesting dominant intrachain antiferromagnetic interactions. Upon further cooling, the $\chi_{mol}T$ increases to a maximum at 3 K, then abruptly decreases at 2 K, with zero-field splitting, Zeeman effects, and weak interchain interactions arising. Similar trends were also observed in ZFC−FC $\chi_{mol}T$ versus T curves at an applied field of 20 Oe (Figure S4 in the Supporting Information). However, the valley of the $\chi_{mol}T$ versus T curve disappears when the applied field is equal to or larger than 1000 Oe. Such a behavior suggests the existence of some

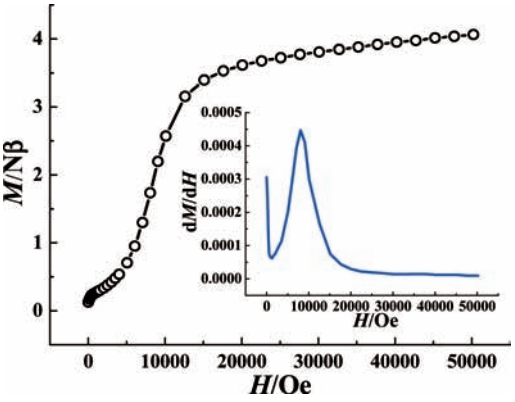

Figure 10. Field dependence of magnetization at 2.0 K for **1**. The dM/dH vs H curve (inset).

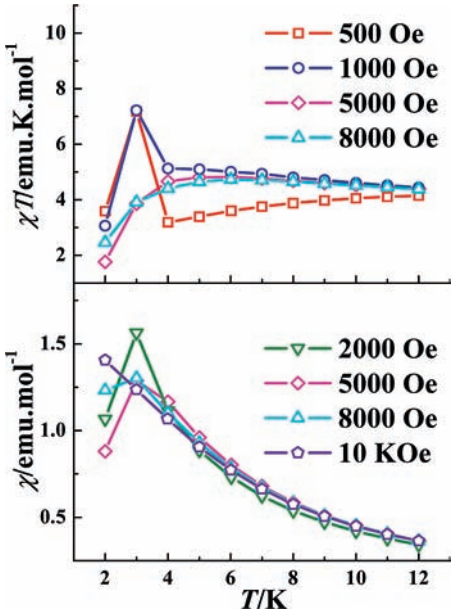

Figure 11. Low-temperature dependence of magnetic susceptibility in the form of χT (above) and χ (below) vs T for **1** at different fields.

field-induced spin canting, which results in the intrachain magnetic interactions changing from an antiferromagnetic into a ferromagnetic state. The field dependence of magnetization measured at 2 K shows a distorted sigmoidal shape. The magnetization of 4.06 Nβ mol^{-1} at 50 kOe is close but does not reach 5.0 Nβ mol^{-1} (Figure 10), the expected saturated magnetization value for the ferromagnetic Mn^{III}−Fe^{III} system with $S_T = 5/2$ (supposing $g = 2.0$), which further confirms the existence of spin-canting. On the other hand, the χ_{mol} versus T curves at fields in the range of above 1000 Oe to below 8100 Oe all display a maximum at around 3 K, revealing the occurrence of an interchain antiferromagnetic coupling. Upon increasing the field, the maximum finally disappears when the applied magnetic field reaches 10 kOe, which overcomes the interchain antiferromagnetic interaction, and another field-induced magnetic transition from an antiferromagnetic to a ferromagnetic state happens. Furthermore, a small hysteresis loop with a remnant magnetization of 0.17 Nβ mol^{-1} and a coercive field of 110 Oe at 2.0 K in a ±10 kOe field (Figure S5 in the Supporting Information) indicates that complex **1** is a soft magnet. The magnetic

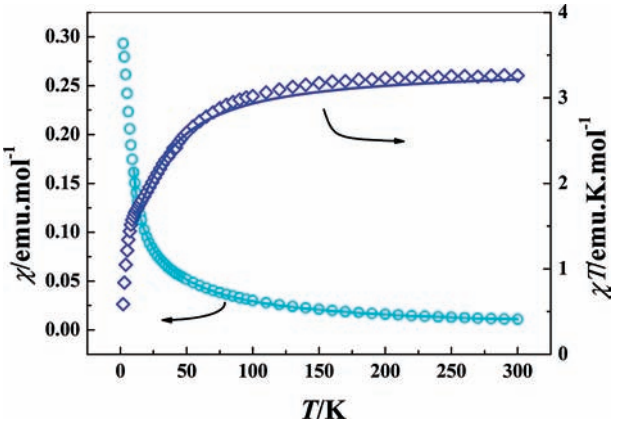

Figure 12. Temperature dependence of magnetic susceptibility in the form of χT (blue) and χ (cyan) vs T for **3** at 1000 Oe. The solid blue lines are the best fitting from 300 to 10 K.

behavior of complex **2** is similar to that of complex **1** because they are a pair of enantiomers (Figures S6−S9 in the Supporting Information). Because a pure 1D system cannot create a long-range magnetic ordering at $T > 0$ K,[1] the interchain interaction is necessary for them to exhibit the spontaneous magnetization.[23] For **1** and **2**, the intermolecular hydrogen-bond weak interactions play an important role in its showing a long-range magnetic ordering through forming a 2D supramolecular array.

The temperature dependence of $\chi_{mol}T$ and χ_{mol} values of complex **3** is displayed in Figure 12. The $\chi_{mol}T$ value is 3.29 emu K mol^{-1} at 300 K, which is slightly lower than the spin-only to the theoretical spin-only value of 3.43 emu K mol^{-1} on the basis of the MnFe unit. As the temperature decreases, $\chi_{mol}T$ gradually decreases, reaching a value of 3.0 emu K mol^{-1} at 100 K. Upon further cooling, the $\chi_{mol}T$ value abruptly decreases to a minimum value of 0.60 emu K mol^{-1} at 2.0 K. Magnetic studies show that complex **3** is a typical antiferromagnetic compound with the intrachain antiferromagnetic coupling between the neighboring cyano-bridged Fe^{III} and Mn^{III} ions. The susceptibility data above 10 K were well-fitted to the Curie−Weiss law, with $C = 3.48$ emu K mol^{-1} and $\Theta = -16.56$ K. The negative Θ value indicates the aniferromagnetic coupling between the Mn^{III} and Fe^{III} ions mediated by the cyanide bridge. The susceptibility data were fitted using the same expression[21a] as for complex **1**, giving $J = -8.0$ cm^{-1}, $g_{Mn} = 2.06$, and $g_{Fe} = 2.12$, with $R = 5.4 \times 10^{-4}$. Again, only data for temperatures above 10 K were considered in the fit to preclude interchain interaction and the zero-field-splitting effect.[22b] The J value is comparable with that of another cyano-bridged $Mn^{III}Fe^{III}$ heterometallic chain-like complex, $[Fe(mpzcq)(CN)_3][Mn(salen)(H_2O)]\cdot H_2O$

(23) (a) Broderick, W. E.; Thompson, J. A.; Day, E. P.; Hoffman, B. M. *Science* **1990**, *249*, 401–403. (b) Kahn, O.; Pei, Y.; Verdaguer, M.; Renard, J. P.; Sletten, J. *J. Am. Chem. Soc.* **1988**, *110*, 782–789. (c) Nakatani, K.; Carriat, J. Y.; Journaux, Y.; Kahn, O.; Lloret, F.; Renard, J. P.; Pei, Y.; Sletten, J.; Verdaguer, M. *J. Am. Chem. Soc.* **1989**, *111*, 5739–5748. (d) Pei, Y.; Kahn, O.; Nakatani, K.; Codjovi, E.; Mathonière, C.; Sletten, J. *J. Am. Chem. Soc.* **1991**, *113*, 6558–6564. (e) Turner, S.; Kahn, O.; Rabardel, L. *J. Am. Chem. Soc.* **1996**, *118*, 6428–6432. (f) Caneschi, A.; Gatteschi, D.; Rey, P.; Sessoli, R. *Inorg. Chem.* **1988**, *27*, 1756–1761. (g) Caneschi, A.; Gatteschi, D.; Renard, J. P.; Rey, P.; Sessoli, R. *Inorg. Chem.* **1989**, *28*, 2940–2944. (h) Yuan, M.; Zhao, F.; Zhang, W.; Pan, F.; Wang, Z. M.; Gao, S. *Chem. Eur. J.* **2007**, *13*, 2937–2952. (i) Liu, C. M.; Zhang, D. Q.; Zhu, D. B. *Inorg. Chem.* **2009**, *48*, 4980–4987.

[mpzcq = 8-(5-methylpyrazine-2-carboxamido)quinoline anion; salen = *N*,*N*′-ethylenebis(salicylideneiminato) dianion), reported quite recently ($J = -6.5$ cm^{-1}).[22b] The field dependence of magnetization measured at 2 K (Figure S10 in the Supporting Information) shows that the magnetization increases gradually with the applied field and reaches a value of 2.28 Nβ mol^{-1} at 50 kOe, which is far from the expected saturated magnetization value 5.0 Nβ mol^{-1}; this feature further confirms the classical aniferromagnetic interaction in **3**. Complex **4** shows a similar magnetic behavior to that of complex **3** because they are a pair of enantiomers (Figures S11−S12 in the Supporting Information).

The structures of enantiomers **3** and **4** are similar to those of enantiomers **1** and **2**, but their magnetic properties are obviously different. The magnetic coupling is determined by the coordination environment and configuration of Fe(III) and Mn(III) ions. To date, most cyano-bridged Mn(III)−Fe(III) complexes exhibit ferromagnetic interactions but with a few exceptions. The Mn−N≡C bond angle seems to play an important role in controlling the magnetic coupling to be ferromagnetic or antiferromagnetic; generally, the bent Mn−N≡C bond angle is unfavorable for the ferromagnetic coupling between d_{z^2} of Mn(III) and d_{xz} of Fe(III).[24] As mentioned above, the average Mn−N≡C bond angle of **3** [147.73(15)°] is much smaller than that of **1** [156.15(4)°], which means **3** has a more bending Mn−N≡C bond angle with respect to **1**, so a classical antiferromagnetic property is expected for **3**. On the other hand, the absence of interchain hydrogen bonds that exist in **1** and **2** seems to be an important reason why **3** and **4** do not display ferrimagnetic properties. The Mn−N≡C bond angle of **1** [156.15(4)°] may be exactly around the critical value required for making the overall magnetic coupling change from a ferromagnetic to an antiferromagnetic state, so **1** displays intrachain antiferromagnetic properties at a low field but ferromagnetic properties at a high field.

(24) (a) Miyasaka, H.; Matsumoto, N.; Okawa, H.; Re, N.; Gallo, E.; Folriani, C. *J. Am. Chem. Soc.* **1996**, *118*, 981–994. (b) Ni, Z. H.; Kou, H. Z.; Zhang, L. F.; Ge, C. H.; Cui, A. L.; Wang, R. J.; Li, Y. D.; Sato, O. *Angew. Chem., Int. Ed.* **2005**, *44*, 7742–7745.

Conclusion

In summary, four chiral cyano-bridged heterobimetallic one-dimensional coordination polymers were prepared by the treatment of $[Fe(Tp)(CN)_3]^-$ or $[Fe(bpca)(CN)_3]^-$ with $[Mn((R,R)\text{-Salcy})(H_2O)_2]^+$ and $[Mn((S,S)\text{-Salcy})(H_2O)_2]^+$, respectively. Complexes **1** and **2** crystallize in the chiral nonpolar space group $P2_12_12$, whereas complexes **3** and **4** crystallize in the chiral polar space group $P2_1$. Complexes **1** and **2** and complexes **3** and **4** are pairs of enantiomers, and the circular dichroism measurements show Cotton effects of the opposite sign at the same wavelengths for each pair of enantiomers. The bending degree of the corresponding Mn−N≡C bond angles and the interchain weak interaction impact the magnetic properties effectively. Enantiomers **1** and **2** display field-induced metamagnetic properties and show an antiferromagnetic long-range ordering with a T_N of 3.2 K, while enantiomers **3** and **4** are typical antiferromagnetic compounds. The polar point group C_2 in which **3** and **4** crystallize is propitious to forming a strongly local dipole, exhibiting an obvious ferroelectric property. This study demonstrates that the magnetic and ferroelectric properties of the chiral cyano-bridged Fe−Mn heterobimetallic one-dimensional chain coordination polymers could be regulated via modifying cyanometalate building blocks. Further investigations on the chiral cyano-bridged Fe−Mn heterobimetallic systems with both ferromagnetism and the ferroelectricity are currently underway in our laboratory.

Acknowledgment. This work was financially supported by the National Natural Science Foundation of China (No. 50662001and 20671093) and the Development Program of Science and Technology of the Education Department of Jiangxi Province (No. 2006-327).

Supporting Information Available: X-ray crystallographic data files (CIF) of complexes **1**−**4** and additional characterization data. The material is available free of charge via the Internet at http://pubs.acs.org.